

Quantum Error Detection with Generalized Syndrome Measurement

Yunzhe Zheng^{1,2,*} and Keita Kanno¹

¹*QunaSys Inc., Aqua Hakusan Building 9F, 1-13-7 Hakusan, Bunkyo, Tokyo 113-0001, Japan*

²*QuTech, Delft University of Technology, Delft 2628 CJ, Netherlands*

(Dated: April 25, 2023)

Quantum error detection has been an experimental focus on early fault-tolerant quantum hardware. However, it requires multiple mid-circuit measurements to extract the syndrome and the readout-induced noise acts as a main contribution to the state infidelity. We present a novel method named *Generalized Syndrome Measurement* for quantum error detection that only requires a single-shot measurement on a single ancilla, while the canonical syndrome measurement needs to measure multiple times to extract the syndrome for each stabilizer generator. Our method minimizes the readout-induced noise by using single-shot measurements with a tolerable overhead on the gate complexity. We simulated the performance of our method using $[[4, 2, 2]]$ and $[[5, 1, 3]]$ code under realistic noise, and our method outperforms the canonical method when the gate error is comparatively small than the readout error. As mid-circuit measurements are more costly for various kinds of near-term scalable quantum hardware, our method can significantly boost the development of early fault-tolerant quantum computing.

Introduction.—Recent experimental progress has demonstrated powerful and scalable quantum computers with different hardware like superconducting qubits [1–7], neutral atoms [8–12] and trapped ions [13–15]. To release the full power of quantum computers, practical quantum hardware need to be made fault-tolerant in order to overcome various kinds of noise and minimize their effect on the quantum states. As a common approach, quantum error correcting codes provide a general framework to tackle noise by encoding a logical qubit into multiple physical qubits [16, 17]. The extra Hilbert space allows the detection and correction of quantum errors, providing the possibility for large-scale fault-tolerant quantum computing.

Due to practical limitations on doing real-time correction, quantum error detection has been a near-term focus for experimental efforts toward early fault-tolerant quantum computing [4, 7, 8, 18, 19] rather than quantum error correction. By post-selecting quantum states depending on the extracted syndrome, we can significantly improve the logical state fidelity under noise without the challenging feedback-control correction. However, canonical syndrome measurement requires multiple mid-circuit measurements to extract the syndrome [20, 21], despite the mid-circuit measurements being a costly operation in current quantum hardware [4, 5]. Even though fast and high-fidelity readout has been demonstrated on isolated qubits [22–25], it remains unclear whether those techniques can be easily extended for more qubits and the readout time length remains much longer than for two-qubit gates as demonstrated in recent scalable hardware. As a result, the whole encoded state will therefore suffer a great amount of decoherent noise when the ancilla qubits are being measured out to extract syndrome. The readout assignment error, i.e. when the qubit is measured

as $|1\rangle$ when being actually $|0\rangle$ or vice versa, also affects the fidelity of the logical state. Therefore, it remains an open question whether there is a method that could reduce the number of measurements for error detection and therefore lower the readout-induced noise.

Here, we propose a novel error detection method, *Generalized Syndrome Measurement* (GSM), that requires only a single-shot measurement regardless of the encoded code size and the number of stabilizer generators. Our method only needs to measure a single ancilla qubit once to extract the code syndrome and thus minimizes the readout-induced infidelity. Our method makes use of the projector gates, which come with a higher circuit complexity as the cost compared with the canonical method. We provide an optimized gate implementation to reduce the gate complexity when decomposed into single-qubit and two-qubit gates. We compared our method with the canonical method under the realistic near-term noisy scenario, and the simulation result shows that our method outperforms the canonical syndrome measurement when the gate error is comparatively small, which falls into the early fault-tolerant setting. As we are stepping into the early fault-tolerant era, our method will thus boost the development of realistic fault-tolerant applications for various quantum algorithms in the near term.

Canonical Syndrome Measurement.—We first give a recap of the canonical method for syndrome measurement (SM). We assume a given quantum error correcting code Q with a k -element stabilizer generator set $\{S_i\}$. Each stabilizer S_i stabilizes quantum states $|\psi\rangle_{in}$ within the codespace Q , i.e.

$$S_i |\psi\rangle_{in} = |\psi\rangle_{in}, \quad (1)$$

and for states $|\psi\rangle_{out}$ outside the $+1$ eigenspace of S_i ,

$$S_i |\psi\rangle_{out} = -|\psi\rangle_{out}. \quad (2)$$

Every stabilizer S_i has an associate projector $P_i = (I + S_i)/2$. An arbitrary quantum state $|\phi\rangle$ can be written as

* dran.z@foxmail.com

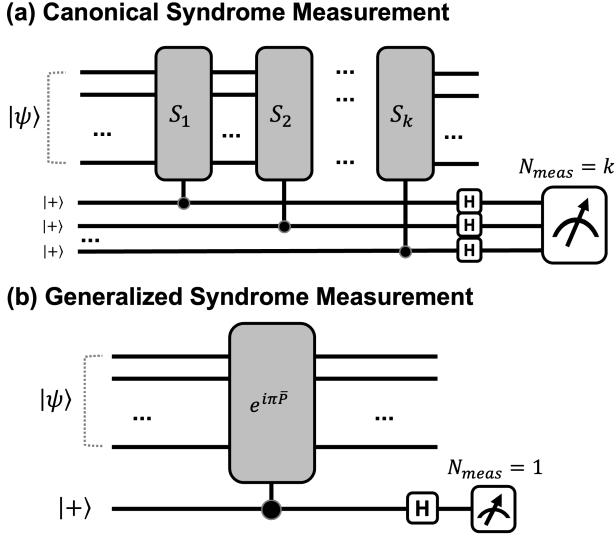


FIG. 1. (a) Circuit scheme for the canonical syndrome measurement. Since each S_i requires a single measurement, the total number of measurements equals the number of stabilizer generators k . (b) Circuit scheme for the generalized syndrome measurement. We apply a control- $e^{i\pi\bar{P}}$ gate between the ancilla qubit and the encoded data qubits. The ancilla qubit will be measured on the X basis to extract the syndrome information. Regardless of the number of stabilizer generators, only a single-shot measurement will be sufficient to detect the error.

a superposition of components in/out of the space defined by S_i ,

$$|\phi\rangle = \alpha|\phi\rangle_{\text{in}} + \beta|\phi\rangle_{\text{out}}, \quad (3)$$

and acting the projector P_i on state $|\phi\rangle$ will eliminate the component out of the code space and correct the noise:

$$P_i|\phi\rangle = \alpha P_i|\phi\rangle_{\text{in}} + \beta P_i|\phi\rangle_{\text{out}} = \alpha|\phi\rangle_{\text{in}}. \quad (4)$$

Nevertheless, P_i is not unitary and cannot be implemented in a quantum circuit directly. Thus, ancilla qubits and additional measurements are employed to achieve a projector on the quantum states as shown in Fig. 1(a). For each stabilizer generator S_i , the canonical syndrome measurement circuit starts with an ancilla qubit in $|+\rangle$ followed by a control- S_i gate controlled by it acting on the data qubits and a Hadamard gate. The whole pre-measurement state is

$$|0\rangle_a P_i|\psi\rangle_d + |1\rangle_a (I - P_i)|\psi\rangle_d, \quad (5)$$

where the subscription a and d stand for the ancilla qubit and the data qubits. Therefore, a +1 outcome measured from the ancilla qubit indicates that the post-measurement state of the data qubits $P_i|\psi\rangle_d$ lies in the +1 eigenspace of S_i . By checking the syndrome of all stabilizer generators, we are able to assure whether the input logical state is within the codespace Q or not. Notice that

although we plot multiple ancilla qubits in Fig. 1(a), usually a single ancilla qubit is reused to reduce the number of required physical qubits.

Generalized Syndrome Measurement.—For the purpose of error correction, the whole syndrome information is useful as feedback-control correction needs to be acted based on it. However, not all syndrome information is valuable for the purpose of error detection. As we only post-select states without any erroneous syndrome, there is no need to distinguish different erroneous syndrome information.

For the code Q , we define the general projector

$$\bar{P} = \prod_{i=1}^k P_i = \frac{1}{2^k} \prod_{i=1}^k (I + S_i). \quad (6)$$

Instead of measuring each stabilizer individually, we aim to detect if a given state is in the codespace or not by a single measurement by using controlled projector gates $e^{i\pi\bar{P}}$. As shown in Fig. 1(b), We started with the noisy input state $|\psi\rangle$ and an ancilla initiated at $|+\rangle$. We apply a control- $e^{i\pi\bar{P}}$ gate triggered by the ancilla state $|1\rangle_a$:

$$\frac{1}{\sqrt{2}}(|0\rangle_a |\psi\rangle + |1\rangle_a e^{i\pi\bar{P}} |\psi\rangle). \quad (7)$$

We then apply a Hadamard gate on the ancilla qubit before measuring the ancilla in the computational basis, and the whole pre-measurement state becomes

$$(|0\rangle_a M |\psi\rangle + |1\rangle_a N |\psi\rangle), \quad (8)$$

where

$$M = \frac{I + e^{i\pi\bar{P}}}{2}, \quad N = \frac{I - e^{i\pi\bar{P}}}{2}. \quad (9)$$

Noticing that \bar{P} is a projector operator and $\bar{P}^2 = \bar{P}$, we have

$$e^{i\epsilon\bar{P}} = I + (e^{i\epsilon} - 1)\bar{P} \quad (10)$$

for any angle ϵ . Therefore, $M = I - \bar{P}$ and $N = \bar{P}$. If we measured the ancilla qubit to be $|1\rangle_a$, the logical state will be projected to state $\bar{P}|\psi\rangle$, which lies in the +1 eigenspace of all stabilizers S_i and therefore in the codespace defined by the stabilizer generator set $\{S_i\}$.

Compared with our method, the canonical SM method achieves the general projector \bar{P} step-by-step, i.e. by projecting P_i sequentially for all stabilizer generators. As a result, at least k measurements are required to detect the error, while our method only requires a single measurement. As mid-circuit readouts are expensive operations for large-scale quantum hardware, we expect our method could significantly reduce the noise originating from measurement.

In addition to the single-shot GSM method, one can also use more ancilla measurements for a reduced gate complexity of the projector gates. As we will show

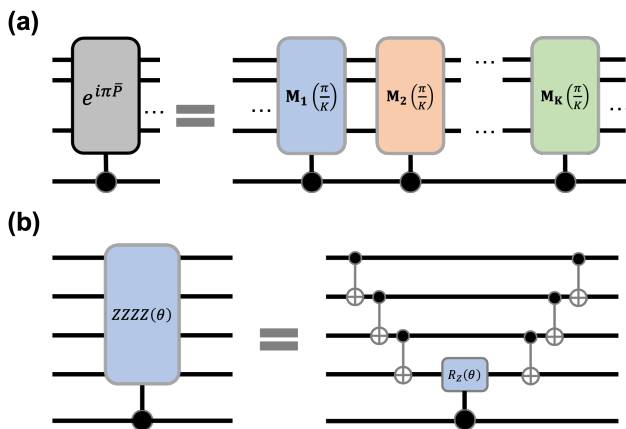


FIG. 2. (a) Decomposed implementation for the controlled projector gates $e^{i\pi\bar{P}}$. This circuit is not final and will be further optimized using Pytket [27]. (b) An example of ZZZZ gate implementation. We decompose the Pauli rotation gate into a V-shape CNOT circuit and control the $R_Z(2\theta)$ gates using the ancilla qubit.

shortly, the gate complexity of the control- $e^{i\pi\bar{P}}$ could be intolerable when the number of stabilizer generators k increases. By making an appropriate trade-off, we can reduce the readout complexity compared with the canonical SM method with a slight gate overhead. This trade-off can be done by splitting the general projector \bar{P} into several subgroups $\{\bar{P}_1, \bar{P}_2, \dots, \bar{P}_m\}$ ($m < k$) such that

$$\bar{P} = \prod_{i=1}^m \bar{P}_i \quad (11)$$

and measuring these subgroup projectors \bar{P}_i separately. As an example, $[[5, 1, 3]]$ code with four stabilizer generators can do a two-shot error detection by choosing $\bar{P}_1 = P_1P_2$ and $\bar{P}_2 = P_3P_4$. We give a detailed explanation in our Supplemental Material [26].

Gate Implementation.—In the canonical method, the control- S_i gates shown in Fig. 1(a) can be implemented using CNOT gates and single-qubit gates. In our method, we demand the implementation for the controlled projector gates $e^{i\pi\bar{P}}$, which are multi-qubit unitary and need to be decomposed into elementary gates to be implemented in real quantum hardware. We expand the expression of \bar{P} in Eq. (6) into a sum of stabilizer operators M_i :

$$\bar{P} = \frac{1}{2^k} \prod_{i=1}^k (I + S_i) = \frac{1}{K} \sum_{i=1}^K M_i, \quad (12)$$

where we define $K = 2^k$ for simplicity. As S_i are stabilizer generators and commute with each other, M_i are also commutable with each other. Thus, an $e^{i\pi\bar{P}}$ gate can be written as

$$e^{i\pi\bar{P}} = \prod_{i=1}^K e^{i\pi M_i/K} = \prod_{i=1}^K M_i(\pi/K), \quad (13)$$

where $M_i(\theta)$ are multi-qubit Pauli rotation gates with angle θ . The projector gates are therefore rearranged in the gate sequences as shown in Fig. 2(a). As the trivial identity gate I is also among M_i , there are actually $K - 1$ gates that need to be considered.

Each $M_i(\theta)$ can be decomposed into a V-shape circuit with only ladder-like CNOT gates mediating qubit interaction and a R_Z gate defining rotation angle θ , up to some single-qubit gates before and after the V-shape circuit [28]. To control the $M_i(\theta)$ gate, we only need to control the $R_Z(\theta)$ gate as the remaining gates will cancel each other if the $R_Z(\theta)$ gate is not triggered. Fig. 2(b) shows an exemplary implementation of the four-qubit Pauli rotation ZZZZ gate.

However, the overall gate complexity is still exponential with the number of stabilizer generators k as $K = 2^k$. To further reduce the gate overhead, we exploit the gate optimization method proposed for the Pauli phase gadgets [27]. For $[[4, 2, 2]]$ code, $S_i = \{XXXX, ZZZZ\}$ and the raw gate implementation requires 21 two-qubit gates. In contrast, the optimized gate implementation requires 13 two-qubit gates, which is only 5 more than the canonical method. For $[[5, 1, 3]]$ code, $S_i = \{ZXZZI, IZXZZ, ZIZXX, XZIZX\}$ and the raw gate implementation requires 105 two-qubit gates. Using gate optimization can reduce the count to 45, 29 more than the canonical method. We can also divide the four stabilizer generators into two subgroups, which results in an optimized implementation with 30 two-qubit gates, only 14 more than the canonical syndrome method. For other common codes and scaling, we have a detailed discussion on the gate complexity in the Supplemental Material [26].

Simulation.—To demonstrate the performance of the GSM method, we use Qiskit [29] to run noisy simulations and calculate the fidelity of the output state after post-selection. We consider depolarizing noise for the gate operations and thermalization (amplitude damping and dephasing) noise for the idling operations and assume all-to-all connectivity. We choose the $[[4, 2, 2]]$ code and the $[[5, 1, 3]]$ code as the examples for demonstration.

We employ noisy encoding circuits to encode a logical state into multiple physical qubits. To model realistic noisy logical states, we insert an idling operation T'_{idle} into all physical qubits after the encoding. We set T'_{idle} to be $3\mu s$ ($8\mu s$) for the $[[4, 2, 2]]$ ($[[5, 1, 3]]$) code simulation. We then separately use the canonical SM method and the proposed GSM method to detect the errors and post-select states without the erroneous syndrome. To model the readout noise, we both consider the readout assignment error and apply an idling operation with duration T_{meas} to all physical qubits for each ancilla readout. For reference, we simulated the fidelity of physical states after idling duration $T_{idle} = T'_{idle} + T_{GSM}$ with T_{GSM} the approximated duration for the GSM method. We have detailed figure illustration in the Supplemental Material for our simulation experiment [26].

For the gate error, we assume the error for the two-

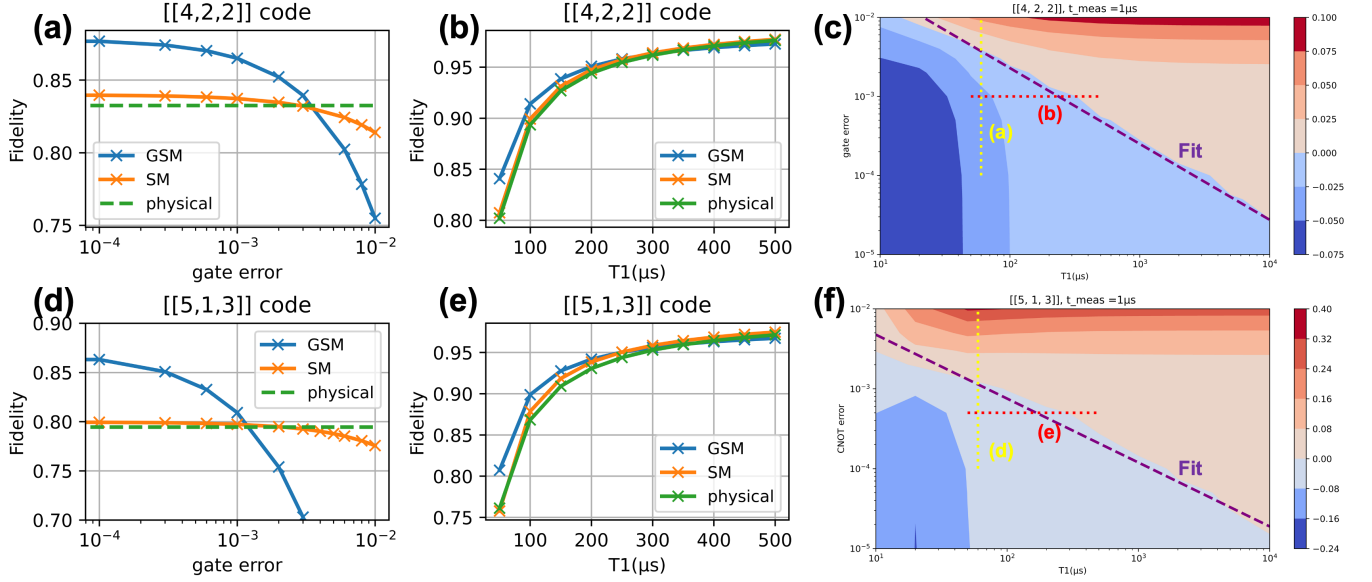


FIG. 3. (a)(d): Output fidelity versus two-qubit gate error rate for $[[4, 2, 2]]$ code and $[[5, 1, 3]]$ code. The coherence time is chosen to be $T_1 = 60\mu s$ and $T_2 = 30\mu s$. (b)(e): Output fidelity versus the coherence time for $[[4, 2, 2]]$ and $[[5, 1, 3]]$ code. We fixed the two-qubit gate error rate to be 0.1% (0.05%) for $[[4, 2, 2]]$ ($[[5, 1, 3]]$) code. (c)(f): Heatmap for $F_{sm} - F_{gsm}$ versus gate error and coherence time for $[[4, 2, 2]]$ and $[[5, 1, 3]]$ code. The range for figure (a)(b)(d)(e) is denoted with red and yellow dotted lines. The purple dashed line is empirically fitted $p_{gate}T_{coh}^{c_1} = c_2$ for the boundary between two methods. For all figures here, we choose $T_{meas} = 1\mu s$ and assumed $T_1 = 2T_2$.

qubit gates is 10 times larger than for the single-qubit gates when varying the error rate. We choose $T_{meas} = 1\mu s$ as the readout duration, which is a state-of-art duration for scalable superconducting hardware [4–6]. A faster readout time can be regarded as a longer coherence time as only the ratio T_{meas}/T_{coh} affects the performance in the simulation. We fixed the readout assignment error rate at 1%.

We first simulated the relation between state fidelity versus the two-qubit gate error with $T_1 = 60\mu s$ and $T_2 = 30\mu s$ uniformly for all physical qubits. As shown in Fig. 3(a) and (d), the GSM method outperforms the canonical SM method when the gate error is comparatively small. For the $[[4, 2, 2]]$ code, the GSM method gains an advantage when the two-qubit gate error is smaller than 0.4%. For the $[[5, 1, 3]]$ code, the GSM method outperforms the canonical method when the two-qubit gate error is smaller than 0.1%. Considering that the best demonstrated two-qubit gate infidelity could reach lower than 0.1% [4], we believe the GSM method will see a practical advantage in the very near future.

We also considered the effect of coherence time on the comparison of the two methods (Fig. 3(b)(e)). We fixed the two-qubit gate error to be 0.1%(0.05%) and $T_1 = 2T_2$ for $[[4, 2, 2]]$ ($[[5, 1, 3]]$) code simulation. When other parameters are fixed, the GSM method will gradually lose its advantage when the coherence time increases. This is because the GSM method gains better fidelity performance by suffering less decoherence induced by the readout, and the decoherence becomes smaller when the

coherence time is longer. For $[[4, 1, 2]]$ ($[[5, 1, 3]]$) code, the two methods have the same simulated performance when $T_1 \approx 400\mu s$ and $T_2 \approx 200\mu s$ ($T_1 \approx 300\mu s$ and $T_2 \approx 150\mu s$). For reference, the current coherence time for scalable superconducting hardware is in the range of 20-50 μs [4, 5].

As the development of quantum hardware could be in parallel for various parameters, we plot a heatmap for the fidelity difference between the two methods $F_{sm} - F_{gsm}$ versus the gate error and the coherence time in Fig. 3(c) and (f). The blue (red) area is where the GSM (SM) has better performance. We also denote the place where we plot the previous figures with dotted lines. We can see the diagonal boundary between the performance of the two methods. The condition when GSM outperforms SM is empirically fitted with

$$p_{gate}T_{coh}^{c_1} \leq c_2, \quad (14)$$

where p_{gate} is the CNOT error, and T_{coh} is the coherence time (T_1) in the unit of μs . c_1 and c_2 are constants that depend on the input parameter of simulation. The constant is $c_1 = 0.96$ and $c_2 = 0.19$ for $[[4, 2, 2]]$ code (Fig. 3(c)), and $c_1 = 0.80$ and $c_2 = 0.03$ for $[[5, 1, 3]]$ code (Fig. 3(f)).

Discussion.—We did not explicitly consider the duration for resetting the ancilla qubits in the simulation for the SM method. Practically, reusing the ancilla qubit actively in a short duration will be challenging due to control difficulty [30]. One can increase the number of ancilla qubits to avoid qubit resetting, which will in turn

lead to a higher cost on the number of physical qubits. We also didn't consider the readout-induced crosstalk effect on the data qubits, which could become a practical infidelity source for near-term hardware. Therefore, we may overestimate the performance of the canonical protocol, and our protocol could bring even better practical advantages than the simulation result in the near term.

We expected the GSM method to have the best usage in the early fault-tolerant setting where quantum error detection is playing the main role. However, our method can also be combined with the canonical method to reduce the readout cost for quantum error correction in the mature fault-tolerant setting. For example, the GSM method can be used for concatenated quantum codes where the low-layer (inner) codes are error-detecting codes. Besides, the GSM method can be used to probe errors in the encoded state before the more expensive canonical syndrome measurement. When the physical error rate is low enough, we have a low probability to detect errors in a single cycle and the generalized syndrome measurement can assure our encoded state is in the code space. We only need to use the canonical syndrome measurement to extract the full syndrome when our method detects the error and the overall number of readout shots will therefore be reduced with the assistance of our method. Nevertheless, as the gates used for GSM are global gates, the error propagated from local physical qubits might serve as the main infidelity. We then need additional methods to suppress the correlated error and we leave the detailed analysis as a future effort.

The parameters used in our simulation are set to be the perspective scalable superconducting hardware in the near-term future. Generally, the GSM method can be applied to various kinds of quantum hardware considering the fact that the mid-circuit readout is mostly expensive for demonstrated hardware so far. For neutral atoms, state-of-the-art scalable mid-circuit readout time is in the scale of tens of milliseconds and the best reachable coherence time is in the scale of hundreds of milliseconds [31]. Particularly, mid-circuit measurement for neutral atoms may rely on coherently transporting the atoms to a separate area as denoted in [8], or may significantly reduce the coherence time by several magnitudes due to control limitation [32]. As two-qubit gates have been demonstrated with over 99.5% fidelity [33], our protocol can therefore be employed to avoid these displeasing overhead and also provide advantages for scalable neutral atoms quantum computers.

We considered the gate complexity using the number of two-qubit gates in this work. Our proposed gate implementation may not be optimal and remains to be further optimized. The gate complexity can also be further reduced using native multi-qubit gates, as demonstrated recently on neutral atoms [12] and superconducting qubits [34] or proposed by using native Ising gates [35].

Acknowledgement.—We thank Johannes Borregaard, Barbara Terhal, Christian Andersen, Masaya Kohda and Yuya O. Nakagawa for insightful discussions. We thank Yanwu Gu, Senrui Chen, Xiaoyu Liu, and Dingshan Liu for proofreading the manuscript.

-
- [1] F. Arute, K. Arya, R. Babbush, D. Bacon, J. C. Bardin, R. Barends, R. Biswas, S. Boixo, F. G. S. L. Brandao, D. A. Buell, B. Burkett, Y. Chen, Z. Chen, B. Chiaro, R. Collins, W. Courtney, A. Dunsworth, E. Farhi, B. Foxen, A. Fowler, C. Gidney, M. Giustina, R. Graff, K. Guerin, S. Habegger, M. P. Harrigan, M. J. Hartmann, A. Ho, M. Hoffmann, T. Huang, T. S. Humble, S. V. Isakov, E. Jeffrey, Z. Jiang, D. Kafri, K. Kechedzhi, J. Kelly, P. V. Klimov, S. Knysh, A. Korotkov, F. Kostritsa, D. Landhuis, M. Lindmark, E. Lucero, D. Lyakh, S. Mandrà, J. R. McClean, M. McEwen, A. Megrant, X. Mi, K. Michielsen, M. Mohseni, J. Mutus, O. Naaman, M. Neeley, C. Neill, M. Y. Niu, E. Ostby, A. Petukhov, J. C. Platt, C. Quintana, E. G. Rieffel, P. Roushan, N. C. Rubin, D. Sank, K. J. Satzinger, V. Smelyanskiy, K. J. Sung, M. D. Trevithick, A. Vainsencher, B. Villalonga, T. White, Z. J. Yao, P. Yeh, A. Zalcman, H. Neven, and J. M. Martinis, *Nature* **574**, 505 (2019), number: 7779 Publisher: Nature Publishing Group.
- [2] M. P. Harrigan, K. J. Sung, M. Neeley, K. J. Satzinger, F. Arute, K. Arya, J. Atalaya, J. C. Bardin, R. Barends, S. Boixo, M. Broughton, B. B. Buckley, D. A. Buell, B. Burkett, N. Bushnell, Y. Chen, Z. Chen, Ben Chiaro, R. Collins, W. Courtney, S. Demura, A. Dunsworth, D. Eppens, A. Fowler, B. Foxen, C. Gidney, M. Giustina, R. Graff, S. Habegger, A. Ho, S. Hong, T. Huang, L. B. Ioffe, S. V. Isakov, E. Jeffrey, Z. Jiang, C. Jones, D. Kafri, K. Kechedzhi, J. Kelly, S. Kim, P. V. Klimov, A. N. Korotkov, F. Kostritsa, D. Landhuis, P. Laptev, M. Lindmark, M. Leib, O. Martin, J. M. Martinis, J. R. McClean, M. McEwen, A. Megrant, X. Mi, M. Mohseni, W. Mruczkiewicz, J. Mutus, O. Naaman, C. Neill, F. Neukart, M. Y. Niu, T. E. O'Brien, B. O'Gorman, E. Ostby, A. Petukhov, H. Putterman, C. Quintana, P. Roushan, N. C. Rubin, D. Sank, A. Skolik, V. Smelyanskiy, D. Strain, M. Streif, M. Szalay, A. Vainsencher, T. White, Z. J. Yao, P. Yeh, A. Zalcman, L. Zhou, H. Neven, D. Bacon, E. Lucero, E. Farhi, and R. Babbush, *Nature Physics* **17**, 332 (2021), number: 3 Publisher: Nature Publishing Group.
- [3] M. Kjaergaard, M. Schwartz, A. Greene, G. Samach, A. Bengtsson, M. O'Keeffe, C. McNally, J. Braumüller, D. Kim, P. Krantz, M. Marvian, A. Melville, B. Niedzielski, Y. Sung, R. Winik, J. Yoder, D. Rosenberg, K. Obenland, S. Lloyd, T. Orlando, I. Marvian, S. Gustavsson, and W. Oliver, *Physical Review X* **12**, 011005 (2022), publisher: American Physical Society.
- [4] Google Quantum AI, R. Acharya, I. Aleiner, R. Allen, T. I. Andersen, M. Ansmann, F. Arute, K. Arya, A. Asfaw, J. Atalaya, R. Babbush, D. Bacon, J. C. Bardin, J. Basso, A. Bengtsson, S. Boixo, G. Bortoli,

- A. Bourassa, J. Bovaird, L. Brill, M. Broughton, B. B. Buckley, D. A. Buell, T. Burger, B. Burkett, N. Bushnell, Y. Chen, Z. Chen, B. Chiaro, J. Cogan, R. Collins, P. Conner, W. Courtney, A. L. Crook, B. Curtin, D. M. Debroy, A. Del Toro Barba, S. Demura, A. Dunsworth, D. Eppens, C. Erickson, L. Faoro, E. Farhi, R. Fatemi, L. Flores Burgos, E. Forati, A. G. Fowler, B. Foxen, W. Giang, C. Gidney, D. Gilboa, M. Giustina, A. Grajales Dau, J. A. Gross, S. Habegger, M. C. Hamilton, M. P. Harrigan, S. D. Harrington, O. Higgott, J. Hilton, M. Hoffmann, S. Hong, T. Huang, A. Huff, W. J. Huggins, L. B. Ioffe, S. V. Isakov, J. Iveland, E. Jeffrey, Z. Jiang, C. Jones, P. Juhas, D. Kafri, K. Kechedzhi, J. Kelly, T. Khatyar, M. Khezri, M. Kieferová, S. Kim, A. Kitaev, P. V. Klimov, A. R. Klots, A. N. Korotkov, F. Kostritsa, J. M. Kreikebaum, D. Landhuis, P. Laptev, K.-M. Lau, L. Laws, J. Lee, K. Lee, B. J. Lester, A. Lill, W. Liu, A. Locharla, E. Lucero, F. D. Malone, J. Marshall, O. Martin, J. R. McClean, T. McCourt, M. McEwen, A. Megrant, B. Meurer Costa, X. Mi, K. C. Miao, M. Mohseni, S. Montazeri, A. Morvan, E. Mount, W. Mruzckiewicz, O. Naaman, M. Neeley, C. Neill, A. Nersisyan, H. Neven, M. Newman, J. H. Ng, A. Nguyen, M. Nguyen, M. Y. Niu, T. E. O'Brien, A. Opremcak, J. Platt, A. Petukhov, R. Potter, L. P. Pryadko, C. Quintana, P. Roushan, N. C. Rubin, N. Saei, D. Sank, K. Sankaragomathi, K. J. Satzinger, H. F. Schurkus, C. Schuster, M. J. Shearn, A. Shorter, V. Shvarts, J. Skrzuzny, V. Smelyanskiy, W. C. Smith, G. Sterling, D. Strain, M. Szalay, A. Torres, G. Vidal, B. Villalonga, C. Vollgraf Heidweiller, T. White, C. Xing, Z. J. Yao, P. Yeh, J. Yoo, G. Young, A. Zalcman, Y. Zhang, and N. Zhu, *Nature* **614**, 676 (2023).
- [5] Y. Zhao, Y. Ye, H.-L. Huang, Y. Zhang, D. Wu, H. Guan, Q. Zhu, Z. Wei, T. He, S. Cao, F. Chen, T.-H. Chung, H. Deng, D. Fan, M. Gong, C. Guo, S. Guo, L. Han, N. Li, S. Li, Y. Li, F. Liang, J. Lin, H. Qian, H. Rong, H. Su, L. Sun, S. Wang, Y. Wu, Y. Xu, C. Ying, J. Yu, C. Zha, K. Zhang, Y.-H. Huo, C.-Y. Lu, C.-Z. Peng, X. Zhu, and J.-W. Pan, *Physical Review Letters* **129**, 030501 (2022).
- [6] S. Krinner, N. Lacroix, A. Remm, A. Di Paolo, E. Genois, C. Leroux, C. Hellings, S. Lazar, F. Swiadek, J. Herrmann, G. J. Norris, C. K. Andersen, M. Müller, A. Blais, C. Eichler, and A. Wallraff, *Nature* **605**, 669 (2022).
- [7] J. F. Marques, B. M. Varbanov, M. S. Moreira, H. Ali, N. Muthusubramanian, C. Zachariadis, F. Battistel, M. Beekman, N. Haider, W. Vlothuizen, A. Bruno, B. M. Terhal, and L. DiCarlo, *Nature Physics* **18**, 80 (2022).
- [8] D. Bluvstein, H. Levine, G. Semeghini, T. T. Wang, S. Ebadi, M. Kalinowski, A. Keesling, N. Maskara, H. Pichler, M. Greiner, V. Vuletić, and M. D. Lukin, *Nature* **604**, 451 (2022).
- [9] K. Singh, S. Anand, A. Pocklington, J. T. Kemp, and H. Bernien, *Physical Review X* **12**, 011040 (2022).
- [10] T. M. Graham, Y. Song, J. Scott, C. Poole, L. Phuttitarn, K. Jooya, P. Eichler, X. Jiang, A. Marra, B. Grinkemeyer, M. Kwon, M. Ebert, J. Cherek, M. T. Lichtman, M. Gillette, J. Gilbert, D. Bowman, T. Ballance, C. Campbell, E. D. Dahl, O. Crawford, N. S. Blunt, B. Rogers, T. Noel, and M. Saffman, *Nature* **604**, 457 (2022).
- [11] A. Omran, H. Levine, A. Keesling, G. Semeghini, T. T. Wang, S. Ebadi, H. Bernien, A. S. Zibrov, H. Pichler, S. Choi, J. Cui, M. Rossignolo, P. Rembold, S. Montanero, T. Calarco, M. Endres, M. Greiner, V. Vuletić, and M. D. Lukin, *Science* **365**, 570 (2019).
- [12] H. Levine, A. Keesling, G. Semeghini, A. Omran, T. T. Wang, S. Ebadi, H. Bernien, M. Greiner, V. Vuletić, H. Pichler, and M. D. Lukin, *Physical Review Letters* **123**, 170503 (2019).
- [13] M. Ringbauer, M. Meth, L. Postler, R. Stricker, R. Blatt, P. Schindler, and T. Monz, *Nature Physics* **18**, 1053 (2022).
- [14] P. T. Dumitrescu, J. G. Bohnet, J. P. Gaebler, A. Hankin, D. Hayes, A. Kumar, B. Neyenhuis, R. Vasseur, and A. C. Potter, *Nature* **607**, 463 (2022), number: 7919 Publisher: Nature Publishing Group.
- [15] C. Ryan-Anderson, J. Bohnet, K. Lee, D. Gresh, A. Hankin, J. Gaebler, D. Francois, A. Chernoguzov, D. Lucchetti, N. Brown, T. Gatterman, S. Halit, K. Gilmore, J. Gerber, B. Neyenhuis, D. Hayes, and R. Stutz, *Physical Review X* **11**, 041058 (2021), publisher: American Physical Society.
- [16] P. W. Shor, *Physical Review A* **52**, R2493 (1995).
- [17] J. Preskill, *Proceedings of the Royal Society of London. Series A: Mathematical, Physical and Engineering Sciences* **454**, 385 (1998), arXiv:quant-ph/9705031.
- [18] C. K. Andersen, A. Remm, S. Lazar, S. Krinner, N. Lacroix, G. J. Norris, M. Gabureac, C. Eichler, and A. Wallraff, *Nature Physics* **16**, 875 (2020).
- [19] N. M. Linke, M. Gutierrez, K. A. Landsman, C. Figgatt, S. Debnath, K. R. Brown, and C. Monroe, *Science Advances* **3**, e1701074 (2017).
- [20] P. Shor, in *Proceedings of 37th Conference on Foundations of Computer Science* (1996) pp. 56–65, iSSN: 0272-5428.
- [21] D. P. DiVincenzo and P. W. Shor, *Physical Review Letters* **77**, 3260 (1996).
- [22] Y. Sunada, S. Kono, J. Ilves, S. Tamate, T. Sugiyama, Y. Tabuchi, and Y. Nakamura, *Physical Review Applied* **17**, 044016 (2022), publisher: American Physical Society.
- [23] J. Heinsoo, C. K. Andersen, A. Remm, S. Krinner, T. Walter, Y. Salathé, S. Gasparinetti, J.-C. Besse, A. Potočnik, A. Wallraff, and C. Eichler, *Physical Review Applied* **10**, 034040 (2018), publisher: American Physical Society.
- [24] D. Reens, M. Collins, J. Ciampi, D. Kharas, B. F. Aull, K. Donlon, C. D. Bruzewicz, B. Felton, J. Stuart, R. J. Niffenegger, P. Rich, D. Braje, K. K. Ryu, J. Chiaverini, and R. McConnell, *Physical Review Letters* **129**, 100502 (2022).
- [25] E. Deist, Y.-H. Lu, J. Ho, M. K. Pasha, J. Zeiher, Z. Yan, and D. M. Stamper-Kurn, *Physical Review Letters* **129**, 203602 (2022).
- [26] “Supplemental material.”
- [27] A. Cowtan, S. Dilkes, R. Duncan, W. Simmons, and S. Sivarajah, *Electronic Proceedings in Theoretical Computer Science* **318**, 213 (2020), arXiv:1906.01734 [quant-ph].
- [28] L. Clinton, T. Cubitt, B. Flynn, F. M. Gambetta, J. Klassen, A. Montanaro, S. Piddock, R. A. Santos, and E. Sheridan, “Towards near-term quantum simulation of materials,” (2022), arXiv:2205.15256 [cond-mat, physics:quant-ph].
- [29] Qiskit contributors, “Qiskit: An Open-source Framework for Quantum Computing,” (2023).
- [30] Y. Zhou, Z. Zhang, Z. Yin, S. Huai, X. Gu, X. Xu, J. All-

- cock, F. Liu, G. Xi, Q. Yu, H. Zhang, M. Zhang, H. Li, X. Song, Z. Wang, D. Zheng, S. An, Y. Zheng, and S. Zhang, *Nature Communications* **12**, 5924 (2021).
- [31] K. Singh, C. E. Bradley, S. Anand, V. Ramesh, R. White, and H. Bernien, *Mid-circuit correction of correlated phase errors using an array of spectator qubits*, Tech. Rep. arXiv:2208.11716 (arXiv, 2022) *****.
- [32] T. M. Graham, L. Phuttitarn, R. Chinnarasu, Y. Song, C. Poole, K. Jooya, J. Scott, A. Scott, P. Eichler, and M. Saffman, “Mid-circuit measurements on a neutral atom quantum processor,” (2023), arXiv:2303.10051 [physics, physics:quant-ph].
- [33] S. J. Evered, D. Bluvstein, M. Kalinowski, S. Ebadi, T. Manovitz, H. Zhou, S. H. Li, A. A. Geim, T. T. Wang, N. Maskara, H. Levine, G. Semeghini, M. Greiner, V. Vuletic, and M. D. Lukin, “High-fidelity parallel entangling gates on a neutral atom quantum computer,” (2023), arXiv:2304.05420 [cond-mat, physics:physics, physics:quant-ph].
- [34] Y. Kim, A. Morvan, L. B. Nguyen, R. K. Naik, C. Jünger, L. Chen, J. M. Kreikebaum, D. I. Santiago, and I. Siddiqi, *Nature Physics* **18**, 783 (2022).
- [35] S. Bravyi, D. Maslov, and Y. Nam, *Physical Review Letters* **129**, 230501 (2022).

Supplemental material for "Quantum Error Detection with Generalized Syndrome Measurement"

Yunzhe Zheng^{1,2,*} and Keita Kanno¹

¹*QunaSys Inc., Aqua Hakusan Building 9F, 1-13-7 Hakusan, Bunkyo, Tokyo 113-0001, Japan*

²*QuTech, Delft University of Technology, Delft 2628 CJ, Netherlands*

(Dated: April 25, 2023)

GENERALIZED SYNDROME MEASUREMENT WITH PROJECTOR SUBGROUPS

In the main text, we introduced the generalized syndrome measurement (GSM) which only requires a single-shot measurement to detect the error. The GSM method requires the ability to implement controlled projector gates $e^{\pm\pi\bar{P}/2}$, which may be a large gate overhead in practical application when the number of stabilizer generators is very huge. Here we propose a method that could reach a smooth trade-off between the gate complexity and the readout complexity.

For code Q with stabilizer generator $\{S_i\}$, the general projector for one-shot GSM method is

$$\bar{P} = \prod_i^k P_i = \frac{1}{2^k} \prod_i^k (I + S_i) = \frac{1}{K} \sum_i^K M_i. \quad (1)$$

As we show in the main text, we can use control- $e^{\pm\pi\bar{P}/2}$ gates and one-shot measurements on the ancilla qubit to act the projector on the noisy state. Instead of using only one projector, we can define multiple subgroup projectors \bar{P}_i such that their product is still \bar{P} :

$$\bar{P} = \prod_i^m \bar{P}_i, \quad (2)$$

where

$$\bar{P}_i = \prod_j^{m_i} P_{i_j} \quad (3)$$

and measure these \bar{P}_i separately using control- $e^{\pm\pi\bar{P}_i/2}$ gates. In this case, The number of readouts is m rather than k for the canonical SM method. For example, we can choose two-element subgroups as $\{S_{2i-1}, S_{2i}\}$, which allows us to define the subgroup projectors \bar{P}_i^2

$$\bar{P}_i^2 = P_{2i-1}P_{2i} = \frac{1}{4}(I + S_{2i-1})(I + S_{2i}), \quad (4)$$

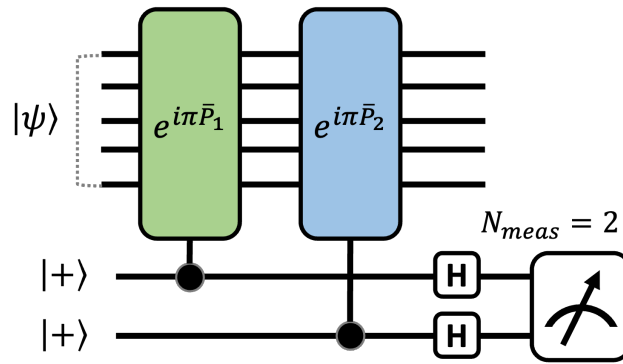


FIG. 1. Circuit scheme for two-shot generalized syndrome measurement for $[[5, 1, 3]]$ code.

and it's easy to see

$$\bar{P} = \prod_i^{k/2} \bar{P}_i^2. \quad (5)$$

We can use the circuit show in the main text Fig. 1(b) to extract the syndrome for each \bar{P}_i^2 . The number of readouts can be halved in this way, and the gate overhead by combining just two stabilizer generators is tolerable. For example, $[[5, 1, 3]]$ code have four stabilizer generators

$$S_1 = ZXXZI \quad S_2 = IZXXZ \quad S_3 = ZIZXX \quad S_4 = XZIZX, \quad (6)$$

the two-qubit gate count to measure \bar{P} with one-shot is 45. Rather if we measure the following two subgroup projectors

$$\bar{P}_1 = \frac{1}{4}(I + S_1)(I + S_2) \quad \bar{P}_2 = \frac{1}{4}(I + S_3)(I + S_4), \quad (7)$$

as illustrated in Fig. 1, we only need 15 two-qubit gates for each subgroup projector and the overall gate overhead is 30.

In general, one is free to group the stabilizer generators. The number of readouts can be chosen smoothly from 1, corresponding to the GSM method proposed in the main text with the largest gate overhead (minimum readout overhead), to k , corresponding to the canonical syndrome measurement with the minimum gate overhead (largest readout overhead).

GATE COMPLEXITY

We present the optimized gate overhead for common stabilizer codes in Table. I. For two-shot GSM for the $[[5, 1, 3]]$ code, as its stabilizer generators are cyclically symmetric, we just pick $\{ZXXZI, IZXXZ\}$ and $\{ZIZXX, XZIZX\}$ as the subgroups and the way how we choose them doesn't affect the gate complexity. For the $[[7, 1, 3]]$ code, we considered two different ways to select subgroups. The first way is to group stabilizers with only X or Z strings, i.e. $\{IIIXXXX, IXXIIXX, XIXIXIX\}$ and $\{IIIZZZZ, IZZIIZZ, ZIZIZIZ\}$, which leads to a two-shot measurement. The second way is to group stabilizers based on active physical qubits, i.e. $\{IIIXXXX, IIIZZZZ\}$, $\{IXXIIXX, IZZIIZZ\}$ and $\{XIXIXIX, ZIZIZIZ\}$, which leads to a three-shot measurement but less requirement for the gate overhead and the connectivity of the physical qubits. We use similar subgroup strategies for the $[[15, 7, 3]]$ code, which is also a quantum Hamming-based CSS code and has stabilizer generators with a similar shape as the $[[7, 1, 3]]$ code.

In general, the gate overhead by using only a single-shot readout for GSM may be intolerable when the number of stabilizer generators scales up. For the $[[n, n-2, 2]]$ error detection code, the gate overhead scales linearly as the code size n . For quantum Hamming-based CSS code $[[2^n - 1, 2^n - 2n - 2, 3]]$, we didn't reach an analytical expression of the gate overhead but one can taste the gate overhead by moving from $[[7, 1, 3]]$ code to $[[15, 7, 3]]$ code. However, it's sufficient to use small-size quantum codes for the early fault-tolerant setting to tackle the noise. Even in the long-term when large-size quantum codes fall into people's focus, one can still achieve a good deal for the trade-off between the readout complexity and the gate complexity by using additional readouts. Therefore, the GSM method will see a practical use for fault-tolerant quantum computation despite the gate overhead.

SIMULATION DETAIL

Fig. 2 shows the circuit used for noisy simulation in our work. For physical qubit, we prepare an ideal state $|\psi\rangle$ and apply an idling operation to it for duration T_{idle} . We set $|\psi\rangle = \cos(\theta)|0\rangle + \sin(\theta)e^{i\phi}|1\rangle$ with $\theta = 0.34\pi$ and $\phi = 0.13\pi$ for the simulation result in the main text. For quantum error detection, we use noisy encoding circuits to prepare a logical state $|\psi\rangle_L$ from $|\psi\rangle$. The detailed encoding circuits can be found in [1, 2]. We then insert an idling operation for duration T'_{idle} to make the input state noisy. We set $T'_{idle} = 2\mu s(8\mu s)$ for $[[4, 2, 2]]$ ($[[5, 1, 3]]$) code. We insert an idling operation for duration T_{meas} to all physical qubits whenever we measure the ancilla qubit as shown in Fig. 2(Middle). We reinitialize the ancilla qubit for the canonical syndrome measurement but didn't explicitly consider the qubit resetting time, which can be incorporated into the readout duration. The fidelity is calculated based on the output multi-qubit noisy state and the ideal encoded multi-qubit state.

Code	SM	GSM	Saved readout	Gate overhead
[[4, 2, 2]]	8	13	1	5
[[$n, n - 2, 2$]](even n)	$2n$	$3n + 1$	1	$n + 1$
[[5, 1, 3]]	16	45	3	29
[[5, 1, 3]](two-shot)	16	30	2	14
[[7, 1, 3]]	24	145	5	121
[[7, 1, 3]](two-shot)	24	62	4	38
[[7, 1, 3]](three-shot)	24	39	3	15
[[15, 7, 3]]	64	573	7	509
[[15, 7, 3]](two-shot)	64	168	6	104
[[15, 7, 3]](four-shot)	64	100	4	36

TABLE I. Two-qubit gate counts comparison between Syndrome Measurement (SM) and Generalized Syndrome Measurement (GSM).

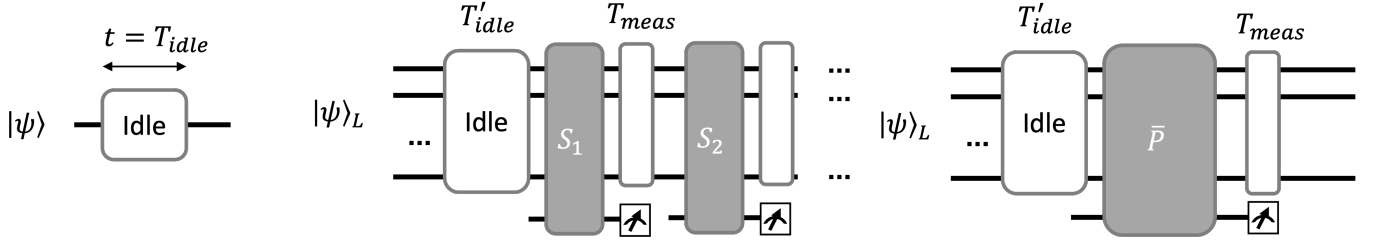


FIG. 2. Simulation circuit illustration for physical (Left), syndrome measurement (Middle), and generalized syndrome measurement (Right). We use both syndrome measurement and generalized syndrome measurement to detect the errors and post select the state without the syndrome. While block stands for idling operations.

In our simulation, we choose $T_{meas} = 1\mu s$. For the simulation of the physical qubits, T_{idle} is chosen such that it's approximately the same as the whole duration for the generalized syndrome measurement: $T_{idle} = T'_{idle} + T_{meas} + T_{gate}$ where T_{gate} is a compensation for the whole gate duration. For the [[4, 2, 2]] code, the two-qubit gate depth is 8 for SM and 9 for GSM. We set $T_{gate} = 1\mu s$ as a rough estimation for the gate duration and we set $T_{idle} = 5\mu s$. For [[5, 1, 3]] code, we set $T_{gate} = 5\mu s$ and $T_{idle} = 13\mu s$. Notice that the choice of T_{idle} only affects the performance of the physical qubit (the green line in Fig. 3 in the main text) and has no impact on the result of (generalized) syndrome measurement.

We plotted the circuit implementation of generalized syndrome measurement in Fig. 3 and Fig. 4, for [[4, 2, 2]] code and [[5, 1, 3]] code respectively.

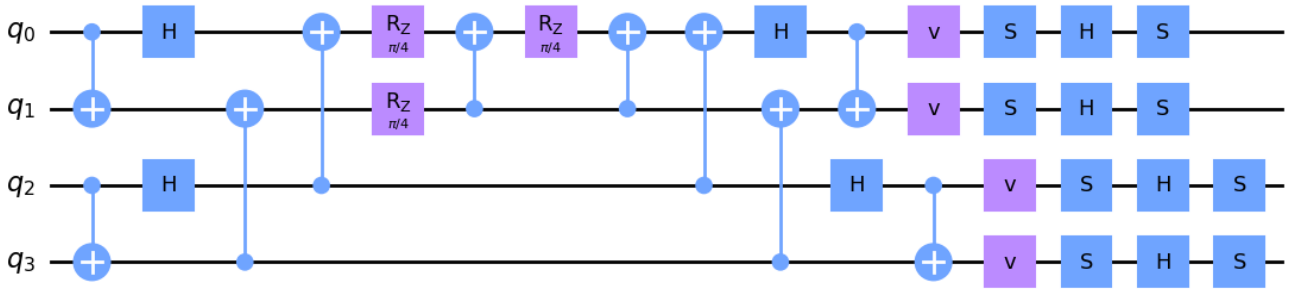


FIG. 3. Optimized GSM circuit implementation of $e^{i\pi\bar{P}}$ for [[4, 2, 2]] code. To control the gate, we only need to control the three R_Z gates.

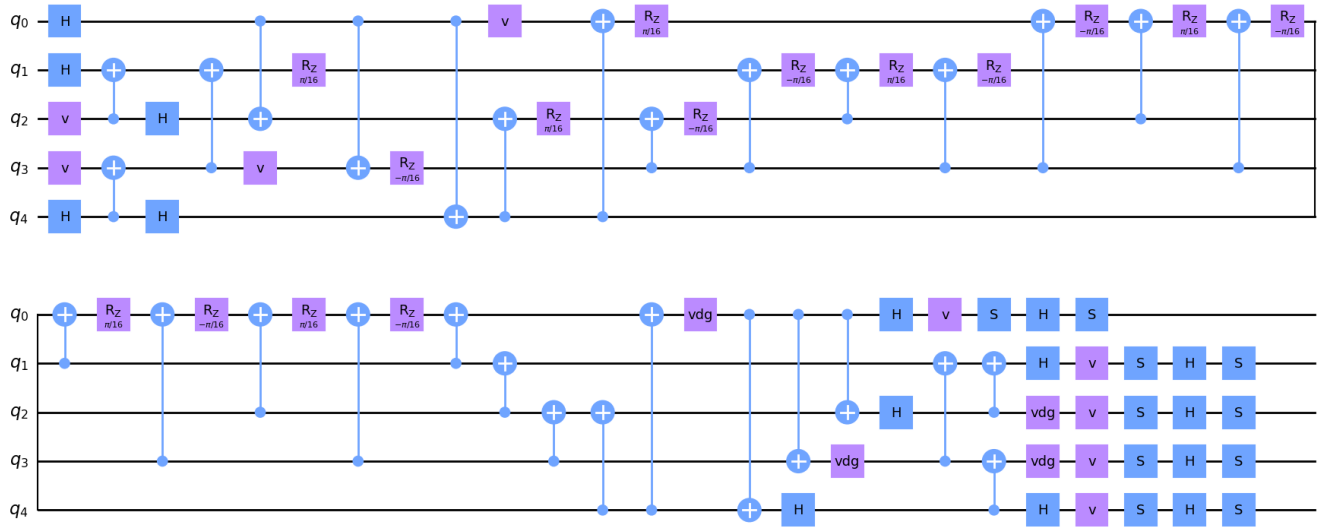


FIG. 4. Optimized GSM circuit implementation of $e^{i\pi P}$ for $[[5, 1, 3]]$ code. To control the gate, we only need to control the 15 R_Z gates.

* dran.z@foxmail.com

- [1] J. Roffe, *Contemporary Physics* **60**, 226 (2019), arXiv:1907.11157 [quant-ph].
- [2] N. D. Mermin, *Quantum Computer Science: An Introduction* (Cambridge University Press, 2007) google-Books-ID: q2S9APxFdUQC.